Auroral alert version 1.0: Two-step automatic detection of sudden auroral intensification from all-sky JPEG images

Masatoshi Yamauchi and Urban Brändström

Swedish Institute of Space Physics, Bengt Hultqvist vägen 1, Box 812, S-98128 Kiruna, Sweden

Correspondence: M. Yamauchi (M.Yamauchi@irf.se)

Abstract. Sudden and significant intensification of auroral arc with expanding motion (we call it "Local-Arc-Breaking" hereafter) is an important event in many aspects but easy to miss for real-time watching due to its short rise time. To ease this problem, a real-time alert system of Local-Arc-Breaking was developed for Kiruna all-sky camera (ASC) using ASC images in the JPEG format. The identification of the Local-Arc-Breaking is made in two steps using the "expert system" in both steps: (1) Explicit criteria for classification of each pixel and simple calculations afterward are applied to each ASC image to obtain a simple set of numbers, or "ASC auroral index", representing the occupancy of aurora pixels and characteristic intensity of the brightest aurora in the image. (2) Using this ASC auroral index, the level of auroral activity is estimated, aiming Level 6 as clear Local-Arc-Breaking and Level 4 as precursor for it (reserving Levels 1-3 for less active aurora and Level 5 for less intense sudden intensification).

The first step is further divided into two stages: (1a) Using simple criteria for R (red), G (green), and B (blue) values in the RGB colour code, and H (hue) value calculated from these RGB values, each pixel of a JPEG image is classified into three auroral categories (from brightest to faintest, "strong aurora", "green arc", and "visible diffuse"), and three non-auroral light source categories ("cloud", "artificial light", and "moon"). Here, strong aurora means that the ordinary green colour by atomic oxygen's 558 nm emission is either nearly saturated or mixed with red colour at around 670 nm emitted by the molecular nitrogen. (1b) The percentage of the occupying area (pixel coverage) for each category and the characteristic intensity of "strong aurora" are calculated.

The obtained ASC auroral index is posted in both an ascii format and plots real-time [1]. When Level 6 (Local-Arc-Breaking) is detected, automatic alert E-mail is sent out to the registered addresses immediately. The alert system started on 5 November, 2021, and the results (both Level 6 detection and Level 4 detection) were compared to the manual (eye-)identification of the auroral activity in the ASC during the rest of the auroral season of Kiruna ASC (i.e., examined all images during total five months until April 2022, and occasionally double checked in the sky). Unless the moon or the cloud blocks the brightened region, nearly one-to-one correspondence between Level 6 and eye-identified Local-Arc-Breaking in the ASC images is achieved within ten minutes uncertainty.

---

[1] https://www.irf.se/alis/allsky/nowcast/

1 Introduction

25 In spaceweather monitoring and real-time studies of the ionospheric/magnetospheric science, real-time broadcasting the monitoring results by web or other method (i.e., nowcasting) of the local geomagnetic and ionospheric conditions, is as important as monitoring the upstream conditions. Here, the upstream condition includes the solar wind and the interplanetary magnetic field (IMF) conditions at the Sun-Earth Lagrange (L1) point, and the detection of the coronal mass ejection (CME) and the solar flare at the Sun. Although the upstream monitor provides predictions of global activities, it is difficult to predict and

30 impossible to know the local geomagnetic and ionospheric activities with the upstream monitor only. This difficulty applies even when the local activity is a part of the predicted global activity such as a substorm: even these cases have uncertainties of at least more than 30 min and several degrees in latitude and longitude. This means that the location and timing of a high geomagnetic and ionospheric activity are difficult to predict by more than these uncertainties, particularly for events with high risk of the spaceweather hazards. For such local forecast, monitoring the local condition (such as the geomagnetic field and

35 all-sky camera (ASC) images) and comparing it with upstream conditions and regional conditions (area covered by several stations) are essential.

Here, aurora condition is known to reflect the magnetospheric and ionospheric conditions (e.g., Akasofu, 1977), and the hazardous magnetospheric/ionospheric conditions almost always cause intense and enlarged aurora. This is why many high-latitude observatories started nowcasting the local auroral conditions (e.g., webcasting the real-time data) after relevant tech-

40 nology becomes ready. Even data from regional network of observations such as geomagnetic array (Friis-Christensen et al., 1988; Luhr et al., 1998) and ASC array (Syrjäsuo et al., 1998; Partamies et al., 2003) are being nowcasted, updating every minute or even more frequent.

Among many traditional methods to monitor the local aurora condition, cost and handiness of ASC decreased drastically during past three decades, making ASC (including those using consumer camera) the most convenient method to monitor the

45 ionospheric condition, although its operation is limited to night. Fig. 1 shows an example of auroral image taken by Kiruna ASC that uses the consumer camera[2]. In addition to the ASC images, some observatories nowcast the keograms of these ASC images using the north-south slices of the images (see Fig. 2 for the explanation of the Keogram). These data are normally archived in the JPEG format with Red-Green-Blue (RGB) colour code (a world-standard image compression format).

Handiness of the ASC data also stimulated non-specialists of the aurora to use the ASC data. These potential users include

50 electric power companies, satellite community (scientists, engineers, and operators) except those engaged with optical instruments, and even tourists and aurora enthusiast. However, these potential users are normally not familiar to interpreting the ASC auroral images nor keograms. For examples, different aurora forms (ratio of different types of aurora) means different magnetosphere-ionosphere current systems for different conditions, such as different UT and different phase of the aurora cycle (about 1-2 hours). Understanding these differences requires background knowledge of relation between various aurora and var-

55 ious magnetospheric/ionosphere activities in addition to actually watching the aurora in the naked eye (Akasofu, 1977). Thus, judging the auroral condition is more demanding than judging the simple morphological difference (existing machine-learning

---

[2]archive is found at https://www.irf.se/alis/allsky/krn/yyyy/
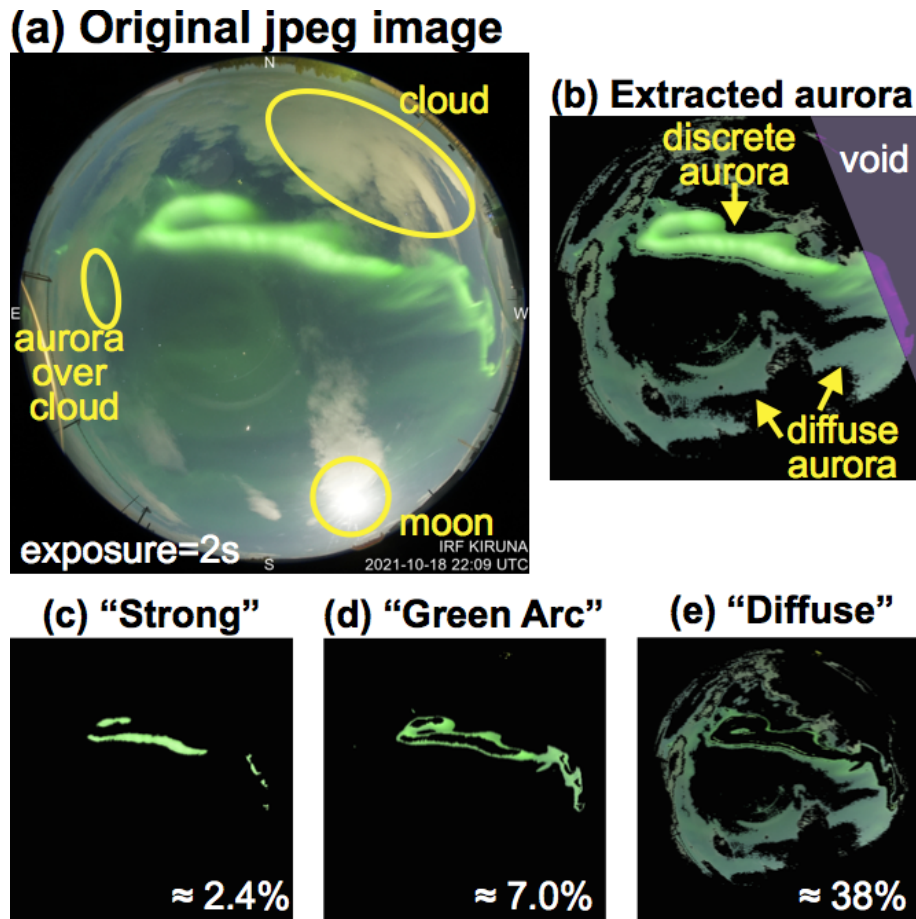
Figure 1. The all-sky image and processed images of 18 October 2021, 22:09 UT, taken by Kiruna all-sky camera (ASC). The automatic exposure time for this particular image is 2 sec (second shortest due to the moon). Aurora pixels are characterized by green colour (its emission is at 558 nm wavelength but that is not resolved in the RGB system). (a) ASC image before the analyses (low-resolution JPEG with 482×482 pixels) that is shrunk from original image (2832×2832 pixels). Basic categories of aurora (discrete and diffuse), cloud, and the moon are marked in the figure. (b)-(e) Processed images by the automatic identification of each pixel (present method), extracting (b) all aurora pixels (window is 430×430 pixels), (c) only "strong aurora" in the present definition, (d) only "green arc", and (e) only "visible diffuse". In the analyses, we mask all pixels more than 215 pixels from the center and also upper right corner (purple-shaded region in (b)) because this part is normally contaminate by the city light (located in the west of ASC).

method has not overcome this problem, see discussion section). Considering wide possible users, it would be ideal if the traditional manual evaluation of auroral activity is translated a numerical scheme and nowcasted, in addition to the keograms.

As the first step of such translation, we define a number representing the size or intensity of each light source (e.g., aurora, moon, cloud). Such a set (short list) of numbers, or namely ASC auroral index, is similar to the geomagnetic indices (obtained

60
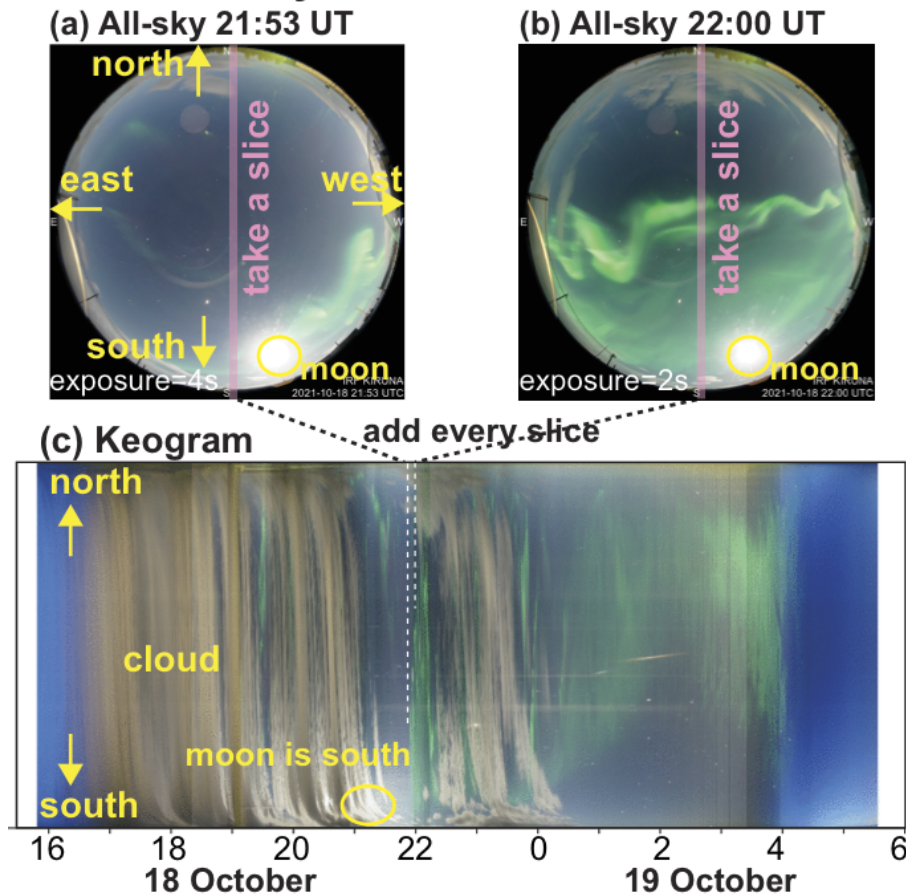
Figure 2. An example of the keogram that is created from a time series of the all-sky camera (ASC) images. Upper panel shows the ASC images during the "Local Arc Breaking" (see text for explanation): (a) 21:53 UT with 4s exposure, and (b) 22:00 UT with 2s exposure. Only the north-south slice of each image (red-hatched area in the middle) is used to create (c) keogram, a time series of the activity (but mixed exposure time as it is) seen in the north-south meridian.

from multi-station data) such as Auroral Electrojet (AE) by the world data center (WDC) in Kyoto[3] for auroral region and Kp by Helmholtz - German Research Centre for Geoscience (GFZ) in Potsdam[4] for sub-auroral region. Another analogy is the moment data (density, velocity, pressure) calculated from particle spectrometer. Such an "index" allows even scientists on aurora to overview the activity during the recent one hour through line plots of the index values.

65   In both the geomagnetic indices and moment values, these simplified "numbers" are used to judge the level of geomagnetic and plasma activities, respectively. Likewise, the ASC auroral index can be used to evaluate the auroral activity level, such as

---

[3]nowcast site: https://wdc.kugi.kyoto-u.ac.jp/ae_real-time/presentmonth/index.html
[4]nowcast site: https://isdc.gfz-potsdam.de/kp-index/

Figure 3. All-sky camera (ASC) at Swedish Institute of Space Physics in Kiruna ($68°$ north).

the sudden and significant intensification of auroral arc with expanding motion (we call it "Local-Arc-Breaking" hereafter). This part is again the translation of eye-identification of the Local-Arc-Breaking (e.g., Akasofu, 1977) into a numerical value. This "second step" classification (judging the activity level from a set of numbers) opens up a possibility of the real-time alert of high activities including the Local-Arc-Breaking. The sequence of aurora shown in Figs. 2a, 2b, and Fig 1a (21:53 UT, 22:00 UT, and 22:09 UT, respectively, on 18 October 2021) is an example of the Local-Arc-Breaking, as characterized by northward quick and expanding motion of the brightest green aurora. The motion is also recognized in the keogram (Figs. 2c). Such real-time alert even allows automatic switch to burst-mode monitoring with higher resolution (e.g., every 5-10 sec instead of every 1 min) to keep the archiving size as small as possible for non-essential period.

In this paper, we describe our numerical translation of manual judge by auroral scientists (expert system) to obtain the Kiruna auroral index and activity level from the all-sky image in Kiruna.

2   Kiruna ASC and source JPEG images

The source data is JPEG images from Kiruna ASC, which is operated by Kiruna Atmospheric and Geophysical Observatory (KAGO) at Swedish Institute of Space Physics (IRF). The ASC is located in a 30 cm heated dome at the roof of the optical laboratory, as shown in Fig. 3, in Kiruna at $68°$ north. The viewing direction of the ASC image is given in Figure 2a. From September 2020, Kiruna ASC uses Sony α7s (firmware rev 3.2) with a Nikon Nikkor 8 mm 1:2.8 objective fish-eye lens with Iris fully open. ISO is set 4000, and colour temperature (white balance) is set 5000 K during the 2021/2022 winter season. The exposure time is dynamic from 1s to about 30s. Like the other standard digital cameras, this camera uses three CCDs with wide spectrum coverage centered at red, green, and blue colours, respectively. The values of detected intensity by each CCD compose the RGB colour code.

The camera is controlled by a Raspberry Pi 4 computer and set to produce RGB colour-coded JPEG files (no raw data output due to storage space limitations), with 2832×2832 pixels in size, out of which a circle with a diameter of about 2700 pixels (about 5.7 million pixels) corresponds to the actual sky window. The data is stored on a disk-server and made available in real time[5]. In addition to the original JPEG files, JPEG files with reduced resolution are also stored in the archive: medium-resolution JPEG (924×924 pixels) and low-resolution JPEG (482×482 pixels).

We use the low-resolution JPEG output, which has a size about the same as those obtained from the old camera (Nikon D700 camera, in service until April 2020). Using the smallest size of JPEG also saves the computation time. Fortunately, the difference in the colour values of each pixel between different JPEG formats (reduced resolution JPEG compared to raw JPEG output from the camera) is much smaller than difference in the colour values between different cameras or during different light conditions (moon, twilight, cloud) according to our experience. This is partly because the JPEG compression well preserves auroral green colour, which is outstanding in the RGB colour space from the other light sources in the night sky.

Since the JPEG format with RGB colour code is commonly used for ASC nowcasting, a successful algorithm for Kiruna ASC may open up a possibility of application (with proper modification) to a wide range of auroral cameras, including those owned by schools and private sectors (e.g., Toyomasu et al., 2008). This would benefit, science (event identification and clarification of physics behind the classification and evaluation), operations (archiving, satellite, spaceweather counterpart), and even education and tourism.

3 Algorithm

As mentioned in the introduction, there are two major tasks: (1) to obtain the ASC auroral index, i.e., a set of numbers representing the sky condition using the colour information of all pixels (about 1.4×10^5 pixels with a 3 byte colour information each), and (2) to evaluate the activity level from this index. A successful result of (1) should make part (2) easy.

The first task is further subdivided into two steps: (1a) We classify each pixel into different categories using mathematical criteria on the RGB values: three categories of aurora ("strong aurora", "green arc", and "visible diffuse", as shown in Fig. 1), non-auroral light sources (cloud, moon, artificial light), and unclassified. To save computation resource, each pixel is classified independently without considering neighbouring pixels' colour, except for judging the moon (white colour occupies a solid small area with radius at least 5 pixels and often about 10 pixels). The classification scheme is detailed in sections 2.1 - 2.3. (1b) We calculate the coverage of each light source and characteristic intensity of the aurora pixels, as described in section 2.4. For the second task (2), we define the activity level, such as the Local-Arc-Breaking, using only the index values, by applying a set of simple criteria, without using any pixel-level information, as described in section 2.5.

To obtain the level, we do not need high digit for the index values, as is the traditional eye-identification of the aurora. Only 1-2 digit of accuracy for the occupancy area in each category (about 50 pixels for strong aurora and about 150 pixels for green arc, according to our experience) is sufficient in defining the activity level. This means that we do not need exact one-to-one relation at pixel level between the actual type of the aurora and classification category. Such tolerance eases the problems

---

[5]https://www.irf.se/sv/observatorieverksamhet/firmamentkamera/

related to the JPEG compression, such as the colour difference of between different JPEG compression schemes from the same image, and only a 3-byte value (1 bytes each for R, G, and B) for colour information in each pixel.

120   The high tolerance also saves computation resource by classifying each pixel independently without considering neighbouring pixels' colour, except for judging the moon (white colour occupies a solid small area with radius at least 5 pixels and often about 10 pixels). Such pixel-level identification of the aurora emission is possible partly because the most outstanding auroral emission for human eye (558 nm) is quite different from other non-auroral emissions in the RGB colour space.

3.1   Selection of auroral colour

125   In version 1.0, we judge only the green aurora (558 nm), which is normally registered as high G values. However, using only the G value in the RGB system is misleading because any bright or while light sources (the moon, artificial light, and cloud reflecting these lights) have a wide spectrum including green colour component, giving high G values. In fact, human eye uses low values in the R/G and B/G ratios in addition to a high G value when distinguishing the green aurora from other light sources in the non-filtered ASC images. We first aim to translate such distinction to a numerical scheme.

130   One useful parameter is hue (H) of hue-saturation-lightness (HSL) colour code that is calculated from the RGB values. We can also use the lightness (L) to set lowest threshold of auroral brightness. Using the calculated HSL values, we actually made primitive version (version 0) of a real-time classification for old ASC (Nikon D700 camera) from November 2016 to April 2020 (see Appendix A for the criteria). Although version 0 could identify many of the Local-Arc-Breaking (Yamauchi et al., presentation at EGU general assembly, 2018), the HSL method causes many identification errors of the aurora pixels for the Sony camera that is in use from August 2020. Therefore, we use all values of R, G, B, calculated H and L.

135

        Note that the H value of an aurora pixel significantly deviates from that corresponding to 558 nm even when the non-auroral emissions are ignorable, partly because other auroral emissions can be mixed. Just limiting to the main emissions, there are three colours that may mix with the green 558 nm emission: several red emission lines around 670 nm corresponding to the nitrogen molecule (N_2 red lines), few blue emission lines near 428 nm corresponding to the molecular nitrogen ion (N_2^+ blue

140   lines), and different red emission line at 630 nm corresponding to the atomic oxygen (O red line). These emissions become strong when the activity is very high, particularly during the Local-Arc-Breaking.

        Among them, the N_2 red line (around 670 nm) is often overlapping with the most intense part of the green aurora (558 nm), with only difference in emission altitude (N_2 red line from < 100 km and oxygen green line from > 100 km), resulting the aurora colour shifting significantly toward red (higher R/G ratio). Similarly, the N_2^+ blue lines increases the B/G ratio (shift

145   the colour toward blue). An example of the ASC image with outstanding N_2 red line is shown in Fig. 4: strong red emissions are found next to (north side of) the main auroral arc in Fig. 4b. The red-white colour between the red pixels and green pixels is the result of both emissions overlapping each other on the same pixel. In this particular case, these pixels are not counted as the (green) aurora pixel simply because R≥G. Fortunately, these lines are intensified only when the green aurora is also intensified, and we can still judge most of such mixed-aurora pixels as "strong aurora" by increasing the criterion values for

150   R/G value or B/G value for higher G ranges. Even the exceptional case like Fig. 4b is normally accompanied by the "strong
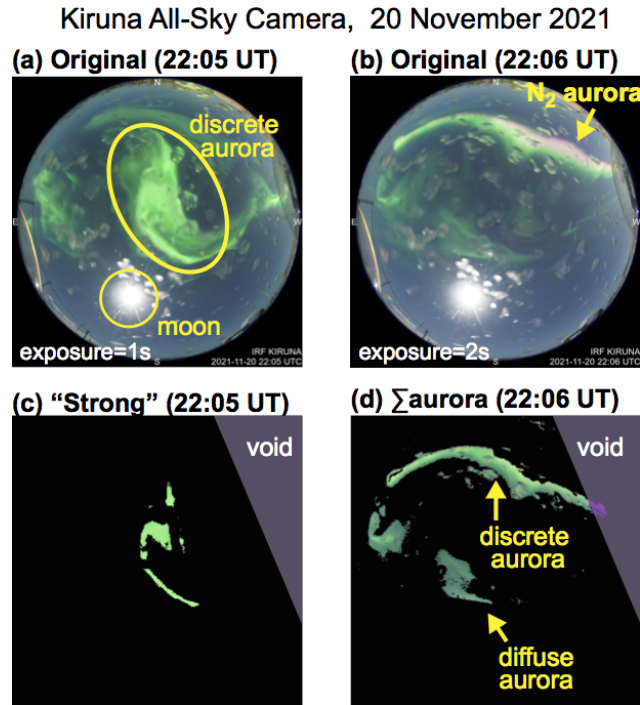
Figure 4. All-sky images of 20 November 2021, at (a) 22:05 UT with 1s exposure, and (b) 22:06 UT with 2s exposure, in the same format as Fig. 1a. (c) and (d) Processed images of (a) and (b) in the same format as 1c and 1b, respectively. The bright spot is the moon, which is removed during the processing.

aurora" on the same image or images ± 1 min as shown in Fig. 4, and does not affect the final evaluation of the auroral activity very much. Therefore, we do not included such strong N_2 red line pixels as the aurora pixels in version 1.0.

There is another factor that affects the colour in the RGB system during very bright discrete aurora that is mainly seen during substorms (e.g., Akasofu, 1977): saturation of G value. In such aurora, non-saturated R and B values increase for higher
155   activity, causing significant increase in the R/G and B/G ratios (while keeping G>R and R>B), and even deviation in the H value. The colour shift (large departure of the H value from that corresponding to 558 nm) also comes from the contamination by non-auroral light sources, particularly the moon and twilight, and the degree of this shift changes with the exposure time (generally shifting to red for longer exposure time).

Fortunately, we may allow tolerance for the pixel-level classification as mentioned above, and handling of such colour shifts
160   is possible. Here, we prioritize the criteria not misjudging the non-auroral source as strong aurora in a critical manner.

3.2   Pixel classification scheme

For the aurora pixel, we define three categories instead of two (discrete and diffuse) because the actual classification is fuzzy and often difficult to judge between discrete and diffuse. We can then define "strong aurora" as clearly discrete one only. The
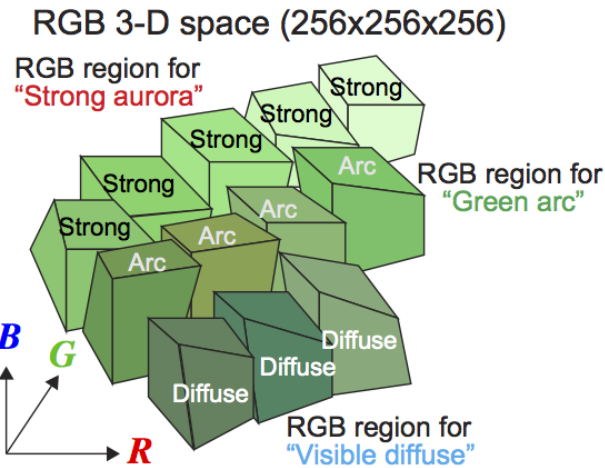
Figure 5. Schematic illustration of how the criteria of aurora pixels are constructed in the RGB colour space. Each small box represents one of many criteria for one category (we call "filter" in this paper) that we consider safe to judge as aurora. By adding these "safe" criteria (with "OR" logic), we can cover wide range of colour (shifted from 558 nm) as the aurora. The block shape is not necessary rectangular because we use G, R/G, B/G, and H in different way for different criteria. The exact conditions are given in Table 2. Such a restrictive definition allows a room to add more pixels to identify as aurora, such as pixels dominated by the N_2 red line (Fig. 4).

green arc category is meant for the discrete aurora with less intensity, and the definition is inclusive because we do not like to
165   miss the discrete aurora from first two categories. Although such definition allows strong diffuse aurora to be misjudged into this category, this error is not critical in detecting the Local-Arc-Breaking because the "strong auroral" is mainly used for this definition. The visible diffuse category is meant for only visible ones while camera can relatively weak diffuse aurora that the naked eye cannot normally recognize. In Fig. 1, the discrete part of Fig. 1a is recognized in Figs. 1c and 1d, while diffuse part of Fig. 1a is recognized in Fig. 1e.

170   Otherwise, the definition is exclusive, i.e., aurora pixels that do not meet these criteria are not included as aurora. We allow such false-positive cases because such a pixel is normally aurora through the cloud or under effect of artificial light and difficult to observe or to use scientific investigation anyway. We even dismissed weak diffuse aurora as "dark" because that is not very important in diagnosing the activity level.

  The exclusive definition is used even when defining the criteria of each category: we add small "safe" areas (we call "filter"
175   hereafter) in the RGB colour space one by one with "OR" logic, as illustrated in Fig. 5. Since the colour balance (H, R/G, and B/G) for the same category changes dynamically and nonlinearly for different G values, we make each filter as restrictive as possible to exclude colours that belong to the other category for the same G values. This method allows us to safely add new criterion in case we miss some colour range for the aurora pixel, while avoiding misjudging non-auroral emissions as aurora. Furthermore, even the strong N_2 red line with very little green line (cf. Fig. 4) can be added as a new category after separating
180   its colour code from the twilight.

Table 1. Example of manual classification and colour values of pixels from an ASC image (18 October 2022 at 22:09 UT, exposure time=2s, Fig 1a)

type	R	G	B	G (%)	H (%)	"filter"[*1]
strong[*2]	171	255	170	100	33.1	N1_995
strong	149	255	155	100	34.2	S1_g95
strong	111	249	128	97.6	35.3	S1_g95
strong	131	242	139	94.9	34.4	S2_g88
strong	112	231	127	90.6	35.6	S2_g88
arc[*2]	95	255	123	100	36.1	A2_H36
arc	61	242	103	94.9	37.2	A2_H36
arc	104	221	130	86.7	36.9	A2_H36
arc	82	188	114	73.7	38.3	A2_H36
diffuse[*3]	54	172	98	67.5	39.4	w2_H36
diffuse	47	158	90	62	39.7	w2_H36
diffuse	50	155	96	60.8	40.6	w5_h40
diffuse	65	109	96	42.7	45	w5_h40
cloud	167	167	129	65.5	16.7	C3_g60
cloud	169	178	157	69.8	23.9	C4_g64
cloud	179	180	138	70.6	16.9	C3_g60
cloud	218	206	168	80.8	12.8	C3_g60
moon	255	255	255	100	0	M_254
moon	244	244	242	95.7	16.7	M_core
moon	226	224	209	87.8	14.7	M_bright
moon	237	235	220	92.2	14.7	M_bright
moon	197	203	201	79.6	44.4	M_full

*1 Each filter means a set of criteria (see Fig. 5) that is defined in Tables 2-4.

*2 Re-construction of "strong", "arc", "diffuse" is shown in Figs. 1c-1e, respectively.

*3 Diffuse aurora is always weak ("w") in naked eye.

The final shape of RGB colour area for the aurora pixels is not smoothly connected, i.e., not completely accurate, as illustrate in Fig. 5. With such uncertainty, some colours simultaneously belong to different categories (e.g., aurora and cloud), while some colours do not belong to any category even if the relevant pixel does not necessarily belong to the clear sky without aurora (such as dark cloud near the edge of the image that does not have enough reflection). However, these uncertainties are not a problem in defining the activity level, for which high tolerance is allowed in the auroral index values as mentioned above.

The exact criteria of the aurora pixels (strong aurora, green arc, visible diffuse) are obtained by manual tuning of the condition. Here, the RGB values of each pixel are extracted after we manually classified the pixel. Table 1 shows an example list of RGB values of pixels for different categories that are manually evaluated (by eye) for Fig. 1a. By examining several

different pixels for the same category, we can make a list of R, G, and B values for one category for one image. This is repeated for different categories (including even Moon, cloud, etc.), different time, different phase of a Local-Arc-Breaking (before, during, and after), different Local-Arc-Breakings, other types of auroral activities, and different days with different conditions (e.g., Moon, cloud, twilight). Once the values are obtained, we also calculate the H, L, R/G, B/G, and (R+B)/G values.

After completing the list for all samples, we arrange the list in terms of G and H values for each category, such that we can tune the condition for other values for given range of the G value (and H value). We prioritize G and H values because these two values are determining factors of "how strong is green" and "how much green", respectively.

3.3 Actual pixel-colour criteria for each category

The result for the Kiruna ASC is given in Table 2 for aurora pixels. The criteria are given with AND logic between column (each column constructs one filter, and named as S1, S2, S3, so on), and then OR logic between rows. The exact values of the criterion are camera-dependent, but the deviation of the values for different camera would generally move toward higher or lower values of R, G, B and therefore the modification will not be very difficult for auroral scientists who actually operates the ASC.

Criteria for pixels with non-auroral emissions are derived in the same manner as for the aurora pixels. Table 3 shows the results for the "moon" and its surroundings, and Table 4 shows the results for the artificial "light", "cloud" without aurora, and "cloud" but possibly under aurora. As mentioned above, the moon body (characterized by high values of all of R, G, B because of its wide colour spectrum) is obtained from the image as a densely populated solid region of pixels (radius at least 5 pixels) that satisfy the moon criterion. We decided not to use the moon location calculated from the time and the moon orbit because the moon location is displaced by the dome, and the moon is often hidden by the cloud, making the part sky covered by the cloud less affected by the moon (main problem of the moon is its effect on the dome rather than on the sky colour).

In these classifications, some pixels meet two or more different definitions. Therefore, we also give a priority order in the following:

1. the moon (Table 3) and artificial light (Table 4),

2. strong aurora (Table 2),

3. green arc (Table 2),

4. visible diffuse (Table 2),

and 5. cloud (Table 4).

The reason for the first priority is to avoid false negative alert (over estimation of aurora pixel) because false negative is more easily occur than false positive. Even with such restrictive definition to avoid false negative, false negative happened as often as false positive from our empirical experience. As compensation, very strong aurora pixels (such as completely saturated with N_2 red line in Fig. 4) can be judged as the moon or the artificial light, but this is a major problem thanks to the high tolerance (allowing 50-150 pixels of misjudge out of about 1.4×10^5 pixels) and reason given at explanation of the N_2 red line.

Table 2. Criteria of a pixel for strong aurora, green arc, and visible diffuse ("strong", "arc", "diffuse" in the first column, respectively)

category	"filter" name[1]	G	H	R/G	B/G	(R+B)/G	R+G+B
strong[2] (with N_2)	N1_995	0.995≤	0.25≤, <0.34	0.50≤, <0.95		<1.90	
strong[2] (with N_2)	N2_97	0.97≤	0.25≤, <0.34	0.50≤, <0.92		<1.90	
strong	S1_g95	0.95≤	0.26≤, <0.36	<0.75		<1.90	
strong	S2_g88	0.88≤	0.30≤, <0.36	<0.70	<0.66		
strong	S3_g83	0.83≤	0.30≤, <0.34	<0.62	<0.57		
strong	S4_g76	0.76≤	0.32≤, <0.36	<0.43	<0.50	<0.89	
strong	S5_g77	0.77≤, <0.83	0.30≤, <0.352	<0.60	<0.64	≤0.96	
strong	S6_g75	0.75≤, <0.95	0.26≤, <0.31	<0.69	<0.54		
arc	A1_H32	0.69≤	0.32≤, <0.36	<0.47	<0.51		
arc	A2_H36	0.69≤	0.36≤, <0.41	<0.70	<0.80		
arc	A3a_H28	0.65≤, <0.80	0.28≤, <0.35	<0.70		<1.21	
arc	A3b_H28	0.65≤, <0.80	0.28≤, <0.35	<0.70	<0.62		
arc	A4_H24	0.59≤, <0.70	0.24≤, <0.27	<0.80	<0.55		
arc	A5_H20	0.59≤, <0.77	0.20≤, <0.24	<0.92	<0.65		
arc	A6_g55	0.55≤, <0.68	0.30≤, <0.36	<0.61	<0.61		
arc	A7_g50	0.50≤, <0.69	0.25≤, <0.35	<0.75	<0.51		
diffuse (+ light)*3	w0_g85	0.85≤, <0.94	0.31≤, <0.38	<0.92	<0.93	<1.83	
diffuse (+ light)*3	w2_H36	0.61≤, <0.80	0.36≤, <0.43	<0.88	<0.92	<1.70	
diffuse	w1_H30	0.61≤, <0.87	0.30≤, <0.36	<0.83	<0.80	<1.60	
diffuse (arc)≤*4	w3_H24	0.40≤, <0.80	0.24≤, <0.31	<0.72	<0.40		
diffuse	w4_H33	0.40≤, <0.65	0.33≤, <0.38	<0.87	<0.90	<1.70	0.98<
diffuse	w5_H40	0.40≤, <0.65	0.40≤, <0.47	<0.72	<0.96	<1.60	0.98<
diffuse*5 (or arc≤)	w6_H18	0.56≤, <0.75	0.19≤, <0.21	<0.95	<0.6		

*1: The name of a filter (a criterion) that can pick up specific colour range of the aurora pixel, and the final criterion for each category is a summation of different filter under "OR" logic.

*2: Contamination from N_2 red line (about 670 nm. see text) increases R/G value.

*3: Contamination by the light is recognized but most likely the visible aurora.

*4: Structured diffuse aurora.

*5: It could be green arc that is reflected by cloud or seen through cloud, but we take safe side not including to the arc.

Fortunately, most of the very strong aurora pixels (e.g., G=1.0) mixed with the other aurora emissions have the H value as 0.24<H<0.34, and are identified as "green arc" or "strong aurora".

The priority order for 2, 3, and 4 is obvious: among all "possibly aurora pixel", we select aurora pixel, and out of them we
225 select auroral arc (the rest is visible diffuse), and from the aurora arc we select strong aurora (the rest is green arc). The cloud

Table 3. Criteria of a pixel for the moon and its surrounding (the same format as Table 2)

category	"filter" name	G	R and G	B and G	
moon	M_254	$G_{255}^{*1} \leq 254$	$R_{255} \leq 254$	$-6 \leq B_{255}-G_{255} \leq 1$	
moon	M_core	$0.95 \leq, <0.997$	$-1 \leq R_{255}-G_{255} \leq 4$	$B \leq G$	$1.95 \leq (R+B)/G <2.01$
near moon	M_bright	$0.70 \leq, <0.97$	$0.994 \leq R/G <1.024$	$0.93 \leq B/G <0.98$	
affected	M_full	$0.60 \leq, <0.90$	$0.79 \leq R/G <0.98$	$0.94 \leq B/G$ & $B_{255}-G_{255} \leq -1$	$0.42 \leq H <0.50$

*1: R_{255}, G_{255}, H_{255} are JPEG value of R, G, B (0-255 instead of 0-1), respectively

Table 4. Criteria of a pixel for the artificial light ("light" in the first column) and cloud (the same format as Table 2)

category	"filter" name	G	H	R/G	B/G	other
light	L1_H45	$0.65 \leq, <0.92$	$0.45 \leq, <0.67$	$0.91 \leq, <1.01$	$0.92 \leq, <1.05$	
light	L2_H39	$0.66 \leq, <0.74$	$0.39 \leq, <0.50$	$0.88 \leq, <0.94$	$0.92 \leq, <1.00$	$1.82 \leq (R+B)/G$
light	L3_H15	$0.66 \leq, <0.74$	$0.15 \leq, <0.19$	$0.94 \leq, <1.01$	$0.96 \leq, <1.00$	
light (+ diffuse)*1	L5_g71	$0.71 \leq, <0.92$	$0.26 \leq, <0.46$	$0.91 \leq, <0.98$	$0.92 \leq, <0.99$	
cloud + light	C1_g995	$0.995 \leq$		$0.995 \leq$	$0.92 \leq$	B<G-0.018 & B<R-0.018
cloud + light	C2_g94	$0.94 \leq, <0.995$	$0.10 \leq, <0.24$	$0.99 \leq$	$0.89 \leq$	B<G-0.018
cloud + light	C3_g60	$0.60 \leq, <0.96$	$0.10 \leq, <0.19$	$0.97 \leq, <1.10$	$0.65 \leq, <0.90$	
cloud + moon	C4_g64	$0.64 \leq, <0.77$	$0.18 \leq, <0.27$	$0.92 \leq, <1.00$	$0.86 \leq, <0.96$	
cloud	C5_g50	$0.50 \leq, <0.67$	$0.10 \leq, <0.20$	$0.95 \leq$	$0.55 \leq, <0.80$	$1.52 \leq (R+B)/G$
cloud	C6_g38	$0.38 \leq, <0.55$	$0.12 \leq, <0.20$	$0.92 \leq$	$0.50 \leq, <0.70$	$1.49 \leq (R+B)/G$
cloud + aurora*2	C7_g41	$0.41 \leq, <0.60$	$0.17 \leq, <0.29$	$0.65 \leq$	$0.50 \leq$	B<R-0.10
cloud + diffuse*3	C8_H26	$0.60 \leq, <0.70$	$0.26 \leq, <0.32$	$0.90 \leq, <0.97$	$0.88 \leq$	
cloud + diffuse*3	C9_H47	$0.55 \leq, <0.70$	$0.47 \leq, <0.55$	$0.80 \leq, <0.95$	$0.95 \leq$	

*1: Similar to note 3 in Table 2, but light effect is stronger than diffuse aurora.

*2: Green arc or strong aurora is above the cloud.

*3: Diffuse aurora is above the cloud.

comes as the last priority because this is for estimating the active area, and thin cloud allows strong aurora to penetrate through. In practise, majority of the cloud criterion does not overlap with the aurora definition.

Related to the moon, there is another problem: the moon modifies the colour toward higher L and higher B/G values at almost all pixels (even aurora pixels far away from the moon) due to the refraction at the dome. This modification is larger at closer pixels to the moon. While better solution for the moon problem (e.g., make the criteria different for different exposure time) will be considered in future, we reduce the moon effect by simply masking all pixels within a certain distance from the moon pixels (14 time of the moon radius that is dynamically obtained) for the present version 1.0. Outside this masked region,

the moon effect is moderate, i.e., the diffuse aurora will never be classified as strong aurora, and even the green arc is not easily be classified as strong aurora.

Of course, such masking may cause underestimation of numbers of pixels of the strong aurora within this masking distance, although eye can identify them. Such a coincidence actually happens because the moon is normally located in the south at which the Local-Arc-Breaking sometimes takes place for the Kiruna ASC. Fortunately, after five months of the real-time operation, the number of missed Local-Arc-Breaking due to this coincidence is small (cf. section 3.5) because the aurora often expands beyond the masked region after the Local-Arc-Breaking (we have enough sample of Local-Arc-Breaking under moonlight). Thus, the present version of dealing with the moon is still effective. Since the moon is characterized by high values of all of R, G, and B, our moon mask would work at other latitude.

We also imposed another mask (void region) in the northwest edge where both the artificial green light source and strong city light is within the field of view, as shaded by purple colour in Fig. 1. Since the light source covers only near the edge of the ASC's field-of-view, we simply remove the entire section from the analyses.

3.4 Calculation of the ASC auroral index

With the classification criteria for each pixel ready (Tables 2-4), we next obtain a set of numbers (parameters) representing the entire image. The obvious parameter is the numbers of pixel, or more precisely, percentage of the coverage over the sky out of about 1.4×10^5 active pixels after removing the void region (cf. Fig. 1b). Since we use fish-eye lens (almost all ASC are using some sort of fish-eye lens), there is a strong geometrical distortions, particularly near horizon. Also, the distance to the emission region (strongest at 100-150 km) is strongly distorted near the horizon. Fortunately, both types of distortion are small near the zenith, and also can be compensated by deploying additional cameras. Therefore, we do not include any correction in the present version (v. 1.0). Including the geometrical effect is one of the future tasks.

The strong aurora (which means near saturation or mixture with the N_2 red lines) is normally identified at a small part of the sky, and the occupancy even during the Local-Arc-Breaking is normally only around 0.5-5% (700 - 7000 pixels, after looking at all plots for the value over 5 months). The green arc occupies a larger area (normally around 1-20% during and before the Local-Arc-Breaking). For reference, strong aurora pixels in Fig. 1 occupy 2.4% (3387 pixels out of 139525 pixel) of the active area of the ASC. Here, Local-Arc-Breaking means obvious expansion of strong area (normally more than double the size within a few minutes). Considering judging error of the strong aurora pixel of about 10% (e.g. Fig 1c compared to Fig 1d), and the artificial green light that can be misjudged as strong aurora is less than 30 pixels, significant digit of 0.03% or 40 pixels for the strong aurora and 0.1% or 150 pixels for the green arc are sufficient in judging the activity level. For the other non-auroral categories, our identification accuracy of the occupied area is much worse, but still we obtain 0.1% significant digit.

The obtained occupancy of the aurora pixels over the sky, however, is not sufficient in evaluating the activity level, because it gives higher values for relatively less luminous aurora with wide area than relatively more luminous aurora with small area within the same category. Another problem is that the brightness given as L values in the HSL colour code (L=(G+min(R,B))/2 for aurora pixels with G>R,B) is not proportional to the photon counts (Brändström et al., 2012; Sigernes et al., 2014). Therefore, we also define the characteristic brightness of the aurora. Here, we do not take a simple summation of L over aurora

Table 5. Content of ASC auroral index

Index content	explanation
%diffuse	occupancy (in %) of visible diffuse pixels
%arc	occupancy (in %) of green arc pixels
%strong	occupancy (in %) of strong aurora pixels (either saturated or N_2 red line is contaminated to the green aurora)
%void	occupancy (in %) of void pixels due to the moon light, artificial light, and obvious cloud that reflects the artificial light
%cloud	occupancy (in %) of specifically the cloud pixels. Note that this is significantly underestimated.
L1	corrected average <L> (luminosity in the HSL) after nonlinear weighting by %arc (and %strong for very small %strong)
L3	corrected average <L^3> after nonlinear weighting by %arc (and %strong for very small %strong)

pixels, because such a summation still gives higher values for wide aurora with low L values than compact aurora with high L values. Instead, we obtain a kind of average intensity of the "strong aurora" pixels, as described below.

If the number of pixels of the strong aurora exceeds 4900 pixels (about 3.5% of the image), we simply use the pixel data for the most luminous 4900 pixels (judged by the L value) among the "strong aurora" pixels. Here, the threshold number can be actually reduced for the present purpose, but it works anyway (as shown in the result below) and does not affect the computation time. Afterward, we use a nonlinear scheme for averaging. We first take the average of both L values and L^3 values. We reduce the obtained average values if the numbers of aurora pixels are small with the coefficient roughly proportional to $1/\sqrt{n_{arc}}$, where n_{arc} is number of pixel of green arc, and zero when strong aurora pixels are less than 10. Here we use L value as representing the luminosity, but we can use G values because what we are counting is intensity of the green (558 nm) aurora. The exact python code is found in the supplemental material.

Table 5 summarizes the obtained parameters for the ASC auroral index. The index values are stored in an ascii file as the csv (comma separated value) format on a website in real-time every minutes[6]. The real-time plot and the archive of the past data are also found on the same website. For the ascii file, we temporally made its width only 72 columns without tab, which makes the file format very similar to the IAGA2002 format of the geomagnetic field. It is quite possible to extend the column to include other key parameter such as the exposure time, moon position and auroral position, but that will be a future task.

Fig. 6 shows an example of comparison between the index values and the keogram over one night (11-12 March 2022). ASC images when the Level 6 activity is detected were also displayed at the bottom. One can see good correspondence with the index values and keogram image.

3.5 Evaluation of the activity level from the ASC auroral index

The next task is to evaluate the activity level from the index values without examining the image data, and then to define the criterion for the activity level that corresponds to the Local-Arc-Breaking (sudden and significant intensification of auroral

---

[6]https://www.irf.se/alis/allsky/nowcast/
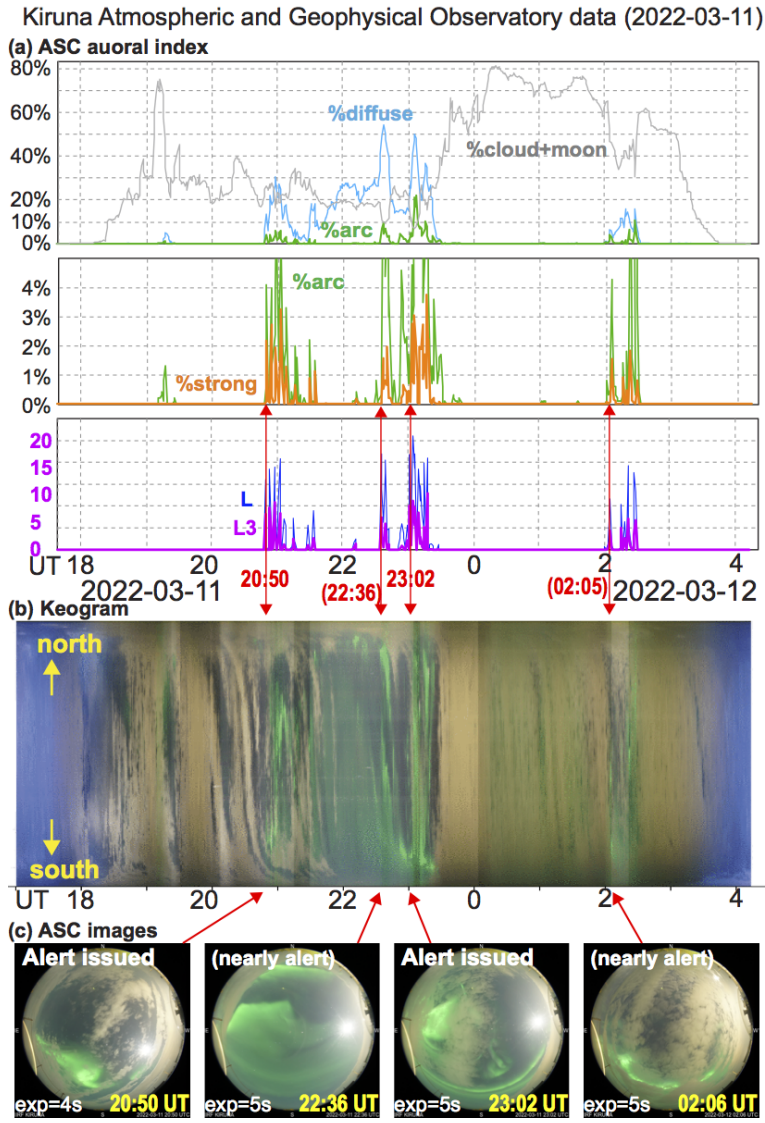
Figure 6. An example of (a) ASC auroral index over one night (11-12 March 2022) with both active aurora and occasional cloud. As reference, (b) keogram over the same night and (c) all-sky images at the time of auroral alert are issued for Level 6 activities. Each image is taken toward the sky with north in the top, and hence east (west) is left (right). All images again include the moon or moon-brightened cloud. The automatic exposure time is 4s or 5s for the displayed images.

arc with expanding motion). Here, the "significant intensification" means high values of L1 or L3 (cf. Table 5), with the "expanding motion" accompanied by more than certain values of "%arc" and "%strong". Table 6 summarizes the criteria for the activity level (Level 6) that most likely corresponds to the Local-Arc-Breaking in the Kiruna ASC. We also defined Level

290

Table 6. Criteria for the activity level (same format as Tables 2-4)

Level	%arc condition	%strong condition	L3 condition
Level 6	$\geq 3\%$ (eventually $\geq 2.95\%$ or 4116 pixels)	$\geq 0.2\%$ (eventually $\geq 0.195\%$ or 273 pixels)	≥ 8 (eventually ≥ 7.95)
Level 4a	$\geq 2\%$ (eventually $\geq 1.95\%$ or 2721 pixels)	$\geq 0.2\%$ (eventually $\geq 0.195\%$ or 273 pixels)	≥ 5 (eventually ≥ 4.95)
Level 4b	$\geq 1\%$ (eventually $\geq 0.95\%$ or 1326 pixels)	$\geq 0.1\%$ (eventually $\geq 0.095\%$ or 133 pixels)	%strong·L3 $\geq 1.5\%$

4a and Level 4b for auroral activity that is close to but less intense than Level 6, as possible conditions for the precursor of Local-Arc-Breaking. Level 5 is reserved for less intense sudden intensification (cf. Appendix B).

Once Level 6 is detected in the real-time ASC image, an alert is sent to the registered mail addresses. We started this alerting system from 5th November 2021. Due to many cloudy nights (particularly during November and December for 2021), Level 6 was detected in limited numbers of nights, but still sufficient to validate this method. In this validation, we examined all ASC images over 5 months by eye (traditional method), and therefore, identification of the Local-Arc-Breaking is somewhat subjective. Although both authors have watched aurora over Kiruna for more than 30 years while one graduate student independently examined the Level 6 warning, the subjective judging problem always remains. Note that this problem also remains with the machine-learning methods because both the sample and results must by validated by eye. We also examined the magnetometer data because it is another (although much less accurate) indicator for the Local-Arc-Breaking (e.g., Akasofu, 1977; Juusola et al., 2020).

Table 7 summarizes the validation results (Level 6 is detected or not, for over one night). The nights when Level 6 was detected are listed for each month until the end of season. Note that from 3 April, the twilight effect makes the detection of Level 6 very difficult and the detection is impossible from 14 April. The bracket [] means the night when the present scheme could not detect the Local-Arc-Breaking in the ASC (i.e., false positive) except those in very north that are difficult to judge.

Unless the aurora brightening takes place very north, above the cloud, or hidden by the moon, the eye-identified auroral brightening is well represented by Level 6 within 10 min. Here, most of the false negative (detection of Level 6 without Local-Arc-Breaking within 10 min) was issued during intensification of auroral arcs before Local-Arc-Breaking or during the expanded auroral activity like substorm expansion phase (Akasofu, 1977), and are related to the same series of aurora activity related to the Local-Arc-Breaking. Only a small fraction of such false negative was un-associated with substantial expansion of the aurora (about 10%).

Likewise, the present method gave small percentage of false positive: The Level 6 auroral activity was not detected 9 nights out of nearly 50 nights with the Local-Arc-Breaking in the ASC. After removing the Local-Arc-Breaking that is affected by moon or twilight, this ratio decrease to 4 night out of about 45 night. Even if we count individual Local-Arc-Breaking when multiple events take place in one night, this low false rate does not change very much. Thus, after 5 month's operation, the Level 6 definition in the present version (version 1.0) works as the event identification purpose for both real-time campaign and statistical studies.

Table 7. List of Level 6 alert during 5 November 2021 - 12 April 2022

month	day[*1]
November 2021	6, 8, 9, 15, [19][*2], 20, [23][*3]
December 2021	5, 6, 19, 21, 27, 31
January 2022:	1, 8, 9, 14, 15, 18, [19][*2], 21, 22, 24, 25, 27, 28, 30, 31
February 2022[*4]	[8][*3], 10, 11, 12, 13,
March 2022	1, 3, 5, 6, [7][*3], 8, 9, 10, 11, [12][*3], 13, [15][*2], 19, 20, 21, 22, 23, 26
April 2022	[3][*5], 7, 12, [14]

*1: Bracket [] indicates that the Local-Arc-Breaking was seen in the image without Level 6 alert.

*2: Moon contamination prevented the identification "strong aurora", with L3=0 for 19 November, L3=6.9 for 19 January, and L3=7.8 for 15 March.

*3: Local-Arc-Breaking in the northern sky only, such that numbers of "strong aurora" did not reach the criterion.

*4: The ASC did not operate on 16-19, and 21 February (total 5 nights).

*5: Relatively weak Local-Arc-Breaking in the dusk sky with some sunlight effect remains, such that exposure time too short to recognize sufficient numbers of aurora pixels.

4 Examples

In this section we show examples of ASC auroral index and ASC images around Local-Arc-Breaking.

4.1 Successful cases

First Level 6 activity after we started the automated mail alert was detected on 6 November 2021, day after we started the system (cloudy on 5 November). Fig. 7a shows the series of Kiruna ASC images around the first Level 6 detection on that day. The ASC auroral index values are given at the bottom of each image. In addition, cloud coverage (in %) is given at the top of each image in Fig. 7a (but not other figures with ASC images). The automatic exposure time (8-10s) is much longer than those of Figs. 1, 2, 4, and 6 (1-5s), partly due to non-moon condition (this is why the city light is outstanding compared to previous images). Each image is taken toward the sky with north in the top, and hence east (west) is left (right).

In Fig. 7a, the Local-Arc-Breaking (most likely the arrival of the auroral substorm bulge to this local time) is seen at 17:31 UT (around 20 MLT) and simultaneously Level 6 is detected, both for the first time in this evening. Before this Local-Arc-Breaking, intensification of the auroral arc equatorward of the original arc was recognized at 17:27 UT (4 min before). In this example, two of three Level 6 conditions, %arc$\geq$3% and %strong$\geq$0.2%, are satisfied from already 17:18 UT, as shown in Fig. 7b, and L3$\geq$8 is the condition that demarcates the activity Level.

As a reference, we also show the geomagnetic variation during this period in Figs. 7c and 7d. Fig. 7c shows fluxgate (DC) magnetometer data **B** and Fig. 7d shows its variation $|\mathrm{d}\mathbf{B}/\mathrm{d}t|$ that is represented by three different methods: simple $|\mathrm{d}/\mathrm{d}t|$ values using 1s resolution data and 10s-running average (still 1s resolution) data, respectively, and the standard deviation divided by square root of 60s ($\sim$7.75s$^{0.5}$), i.e., normalized fluctuation over 60s. At 17:31 UT when the auroral brightening reached to Level 6, the geomagnetic field suddenly changed, with B$_X$ started changing by more than 100 nT within a minute
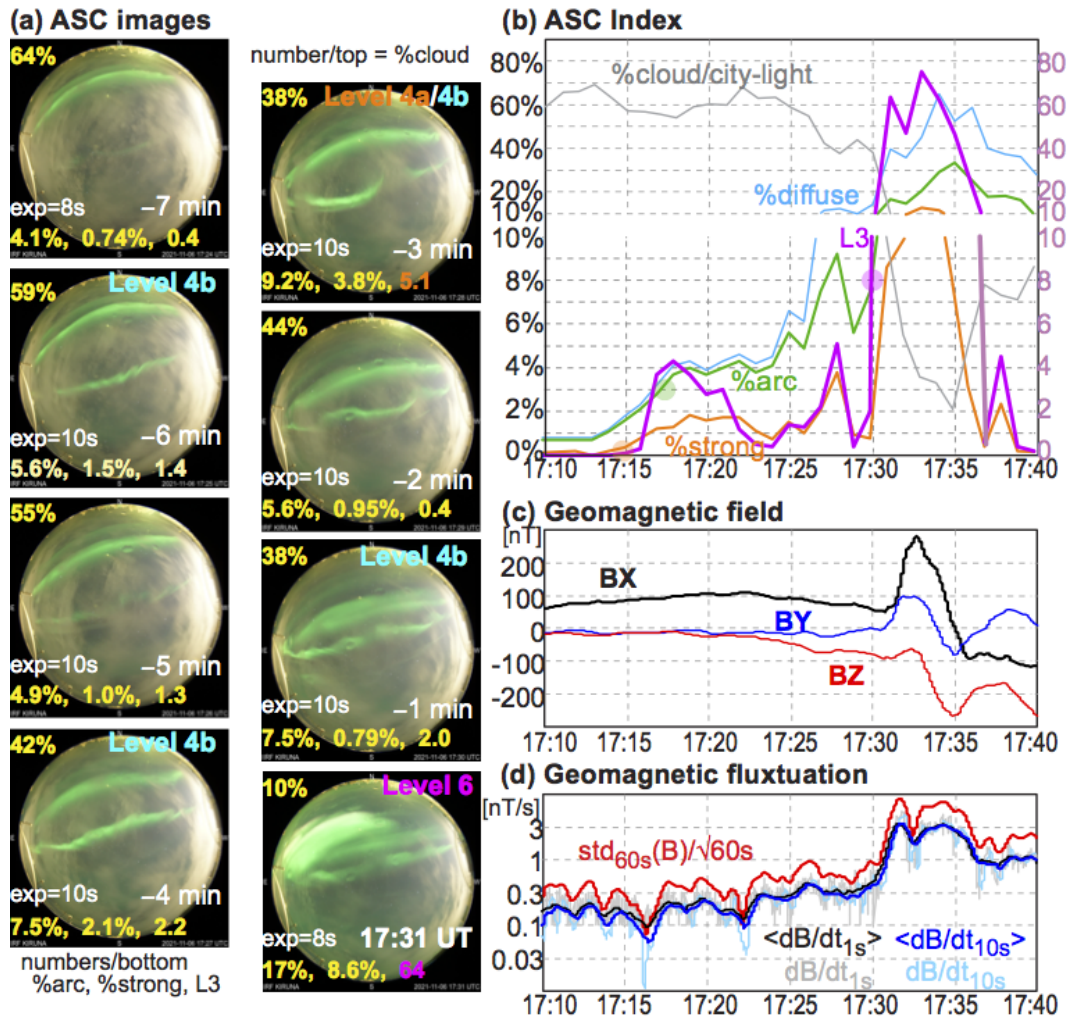
Figure 7. ASC and magnetometer data around 17:31 UT on 6 November 2021:(a) Auroral images (the same coordinate as Fig. 2); (b) ASC auroral index values; (c) DC geomagnetic deviation from the baseline values (X=north, Y=east, Z=downward); and (d) AC geomagnetic variation |dB/dt| measured by three different methods. In each image, the ASC auroral index values of %arc, %strong, and L3 are given at the bottom, above which the automatic exposure time and UT are given. The cloud coverage (%cloud) and the activity level (Level 6, Level 4a, and Level 4b) are given at the top. The timing of Level 6 detection is the same as the onset of the Local-Arc-Breaking. In the auroral index panel (b), the scaling is changed between below 10 and above 10 (therefore the graph has a gap in between). The three methods of |dB/dt| are: (1) using 1-sec values (black), (b) using 10 sec running average values (blue), respectively, and (3) standard deviation of magnetic field over 60 sec using 1-sec values and normalized to nT/s unit (red). These variations are first calculated for each vector component, and then taken the absolute values.
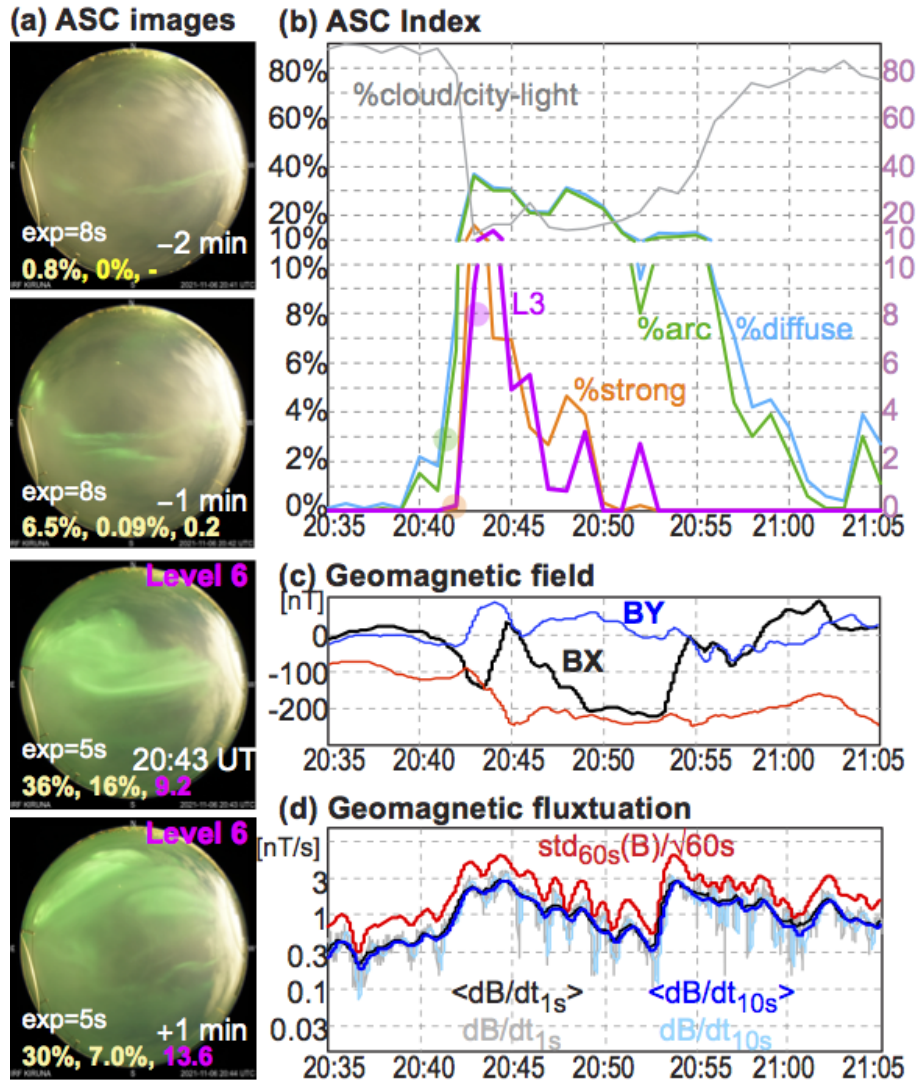
Figure 8. The ASC images, ASC auroral index values and geomagnetic data around the time when the Level 6 aurora activity was detected at 20:43 UT on the same night as Fig. 7. The format is the same as Fig. 7 except that the cloud coverage is not shown on the ASC images.

(this satisfies necessary condition of a substorm) while magnetic deviation increased by an order of magnitude in all three methods.

The next detection of Level 6 activity was under more cloudy condition at 20:43 UT (around 23 MLT) on the same day. Fig. 8 shows the series of Kiruna ASC images, time series plots of the ASC auroral index values and geomagnetic activities in the same format as Fig. 7 except that the cloud coverage is not given on the ASC images. The automatic exposure time (8s and 5s)
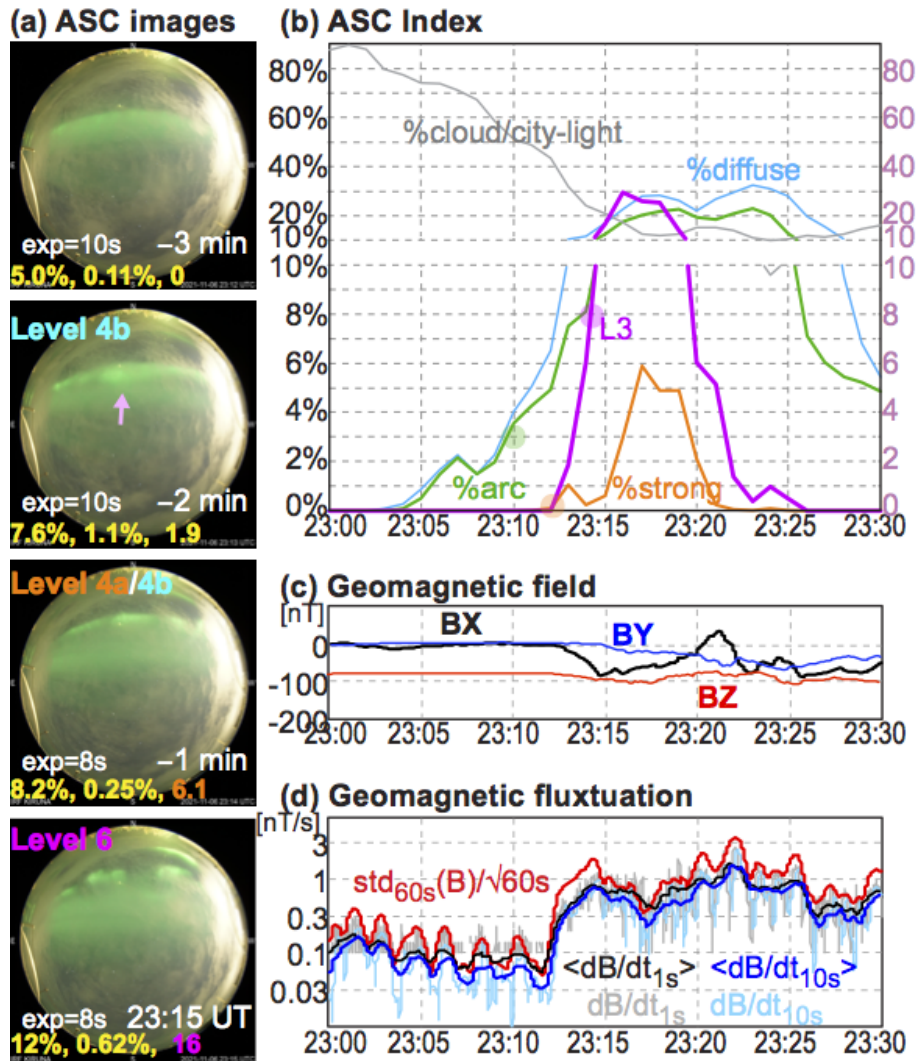
Figure 9. The same as Fig. 8 for the Level 6 auroral activity at 23:15 UT on the same night as Figs. 7 and 8.

is the same as or slightly shorted than those of Fig. 7. Due to heavy cloud coverage (almost full coverage over the sky), auroral arc before the sudden and significant intensification was not well recognized until one minute before (20:42 UT), at which only one parameter (%arc) reached the criterion of Level 6, while other parameters (%strong and L3) did not reach the criterion of Level 4a or 4b. Fortunately the cloud was not very thick and the brightening of aurora was strong enough to be recognized in the ASC auroral index. The timing of Level 6 detection (20:43 UT) again corresponds to a large geomagnetic deviation with more than 100 nT change in B_X and nearly one order of magnitude increase of the magnetic deviation in all three methods.

345

In both examples (17:31 UT and 20:43 UT), Level 6 detection timing agrees with the timing of the Local-Arc-Breaking in the ASC image, and the morphology the Local-Arc-Breaking is consistent with the evening auroral surge during a substorm (Akasofu, 1964). The last detection of the Level 6 activity on the same night at 23:15 UT took place in the post-midnight sector (around 01 MLT). Fig. 9 shows the relevant images and plots in the same format as Fig. 8. The automatic exposure time (8-10s) is the same as those of Fig. 7. In this example, the aurora brightening started already at 23:13 UT, two minutes before the Level 6 detection, as is also indicated by the geomagnetic deviation (90 nT change of the X component in 2 minutes). Instead of Level 6, ASC auroral index values gave Level 4b at 23:13 UT, and Level 4a at 23:14 UT (%arc=8.2%, %strong=0.25%, and L3=6.1). The magnetic deviation also increased significantly, but the peak values are much lower than previous Level 6 activities (Figs. 7 and 8) by more than a factor of 3. Considering such a small geomagnetic activity and its post-midnight location, two minutes delay of Level 6 detection is still successful for the real-time alert.

Since the morphology and intensity the aurora are quite different between the pre-midnight and post-midnight (e.g., Akasofu, 1964), the relation between the ASC auroral index and the auroral intensification must also different between them. For example, diffuse aurora in the post-midnight is often registered as green arc because of its high intensity. Ideally, different criteria should be used between pre-midnight and post-midnight. On the other hand, the present algorithm anyway detects the Level 6 for many of post-midnight cases because the criterion the L3 value is not very much affected. This is why we keep the consideration of the local time as a future task but not very urgent.

4.2 Moon effect

Here, we show two examples with strong influence by the moon: one successful case (15 November 2021, 20:36 UT) in Fig. 10 and one unsuccessful case (19 January 2022, 23:57 UT) in Fig. 11. The examples with the moon in Figs. 1 and 2a also satisfy the Level 6 criterion, and the examples of the Local-Arc-Breaking in Fig. 6 (20:50 UT and 23:02 UT) also satisfy the Level 6 criterion. In Fig. 10, Level 6 was detected at 20:36 UT, which is only 2 minutes after some signature of the Local-Arc-Breaking becomes visible in the ASC. The automatic exposure time (4s) is the same as that in Fig. 2a and similar to those in Fig. 6c, both with the moon. For this event, the brightened aurora is located very close to the moon, and that caused relatively low L3 values and low %strong values. Nevertheless, values of the ASC auroral index reached to Level 6. Comparing to the local magnetometer data (Figs 10c and 10d) that indicate the Local-Arc-Breaking at 20:39 UT, the ASC auroral index gave closer time to the Local-Arc-Breaking.

In the unsuccessful case (Fig. 11), the peak L3 value was only 6.9 at 23:57 UT although the ASC image shows the Local-Arc-Breaking some distance north from the moon. The automatic exposure is shortened to 2s, the same as those with the moon in Figs. 1a and 2b. Both the geomagnetic deviation (> 150 nT within 5 minutes) and the magnetic variation reaching nearly 3 nT/s one minute after at 23:58 UT (same level as of Figs. 7, 8, and 10) indicates that aurora activity corresponds to the Local-Arc-Breaking. With %arc =7.0% and %strong =0.41% at this time, only the L3 value did not reach the Level 6 criterion.

The small L3 value must be mainly due to reduced exposure time by the existence of the moon, but might also come from wide refraction of moonlight through the dome that also changes the colour (H value) of the aurora pixels. As the result, even colour in background pixels (night sky) become more bluish than the case on 6 November 2021. We consider the colour shift
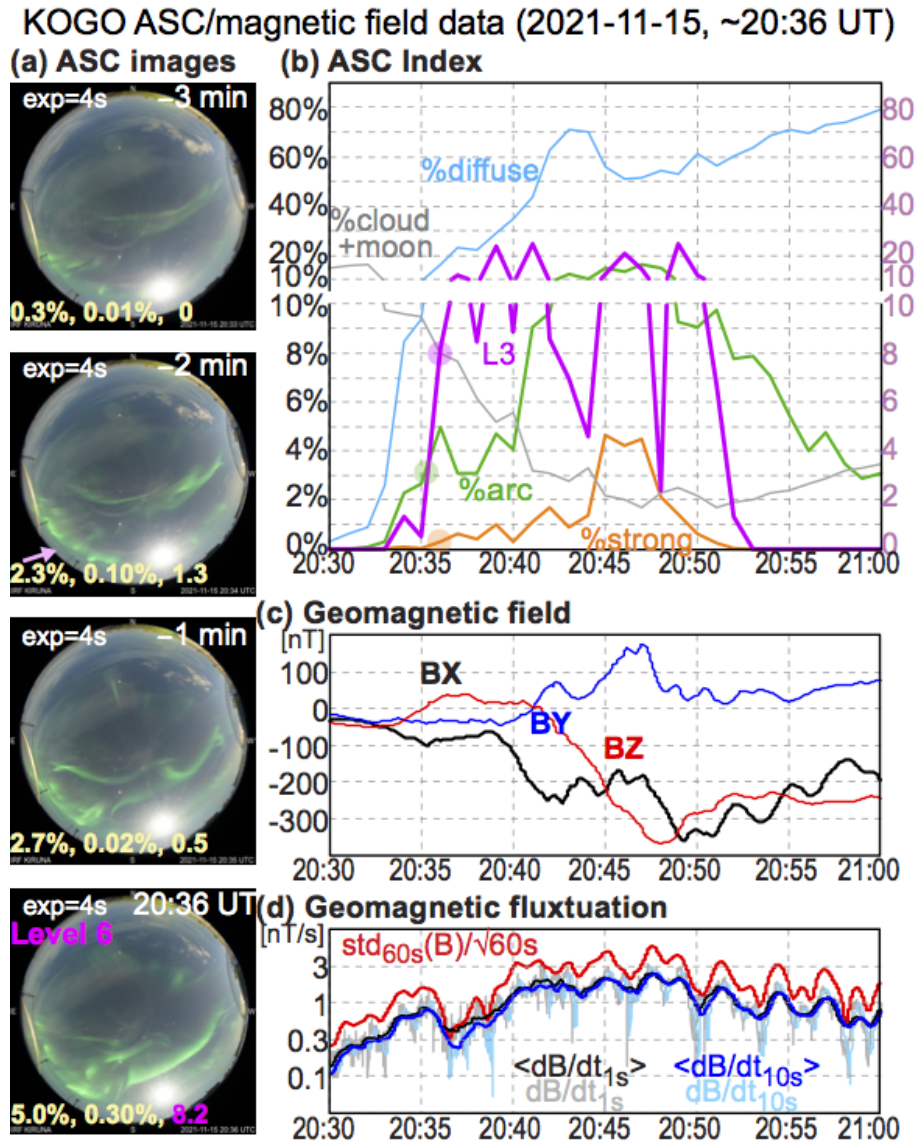
Figure 10. The same as Fig. 8 for the Level 6 auroral activity at 20:36 UT on 15 November 2021.

important because next example (Fig. 12) with longer exposure time is also unsuccessful. Taking care of these problems is one of the future tasks.

4.3 Twilight effect in spring and fall

385   Like the moon effect case, twilight case also changes the colour of the entire image toward blue. Fig. 12 shows one such unsuccessful case. The automatic exposure time (4-5s) is similar to those of the successful moon cases (Figs. 6 and 10). A
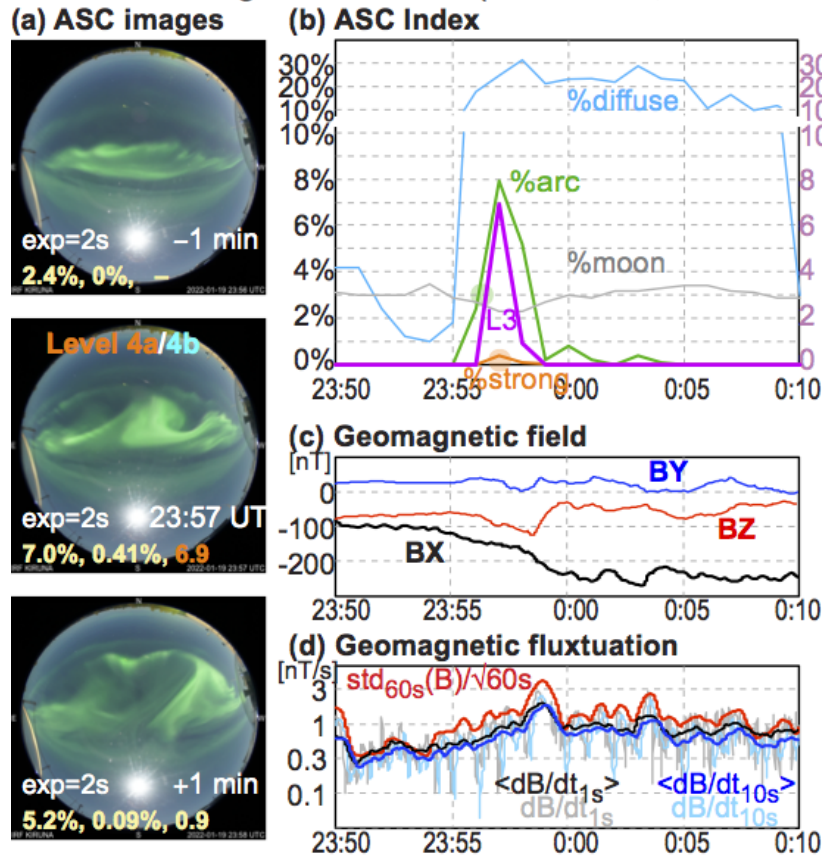
Figure 11. The same as Fig. 8 for the Level 4a/4b auroral activity at 23:57 UT on 19 January 2022.

clear Local-Arc-Breaking took place in the northern sky. In fact the L3 value exceeded the Level 6 criterion at 20:06 UT and 20:07 UT. However, the aurora coverage (either %arc or %strong) did not reach the needed values (marked by blue circle in the figure). Thus, the short exposure time alone does not prevent the ASC auroral index reaching to Level 6.

4.4 Missed case due to northward auroral location

If the Local-Arc-Breaking takes place in the northern sky with large zenith angle, geometric effect (cf. section 3.4) reduces the aurora coverage (%arc and %strong). This sometimes prevents detection of the Local-Arc-Breaking, particularly for relatively weak ones. Fig. 13 shows one such example of the Local-Arc-Breaking in the far-north part of the field-of-view (23 November 2021, 21:28UT) without reaching Level 6 due to too small auroral coverage. The automatic exposure time (3-4s) is within the range of successful cases shown in Figs. 1, 10, and 11, thanks to a thin cloud reducing the moon effect. The brightest image was taken at 21:29 UT with sufficient %strong (=1.15%) and L3 (=9.5) for Level 6, but %arc (=1.9%) was far below the required threshold ($\geq 3\%$) for Level 6 (marked by blue circle in Fig. 13a). The geomagnetic deviation (Fig. 13c) of more than
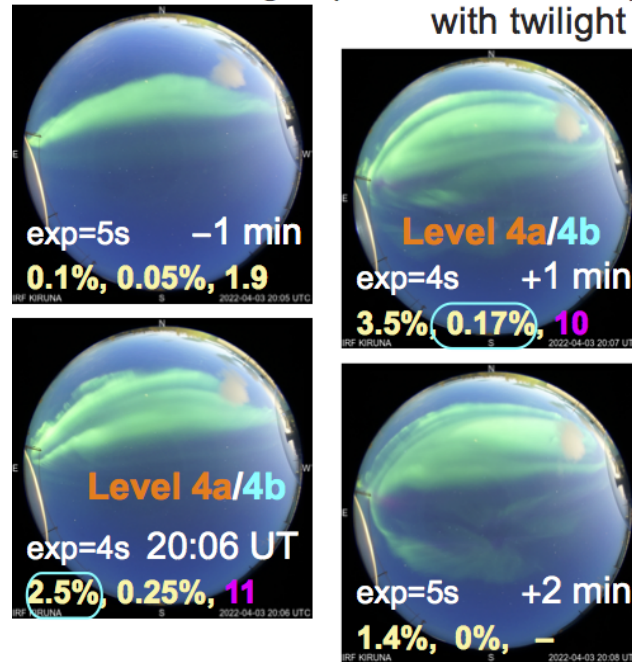
Figure 12. ASC images around 20:06 UT on 3 April 2022, when the ASC auroral index values did not reach Level 6 due to the twilight effect when the Local-Arc-Breaking took place.

Table 8. Summary of examples

Problem	Solution	Reference
thin cloud	Level 6 works	Fig. 8
precursor	Level 4 is good canddate	Figs. 7 and 9
post-midnight	Level 6 works	Fig. 9
geomagnetic signature	$\Delta B > 100$ nT & $|dB/dt| > 2$ nT/s	Figs. 7-10
different exposures	Level 6 works	Figs. 7-10
Moon effect	bluish colour & short exposure	Figs. 10-11
twilight effect	bluish colour & short exposure	Fig. 12
northern sky	too small area	Fig. 13

100 nT, and geomagnetic variation (Fig. 13d) of about 1-3 nT/s are, considering aurora location far north that causes reduced geomagnetic signatures, large enough to be accompanied by a Local-Arc-Breaking.

400  Table 8 summarizes the features and problems that are explained in the examples Figs. 7-13.
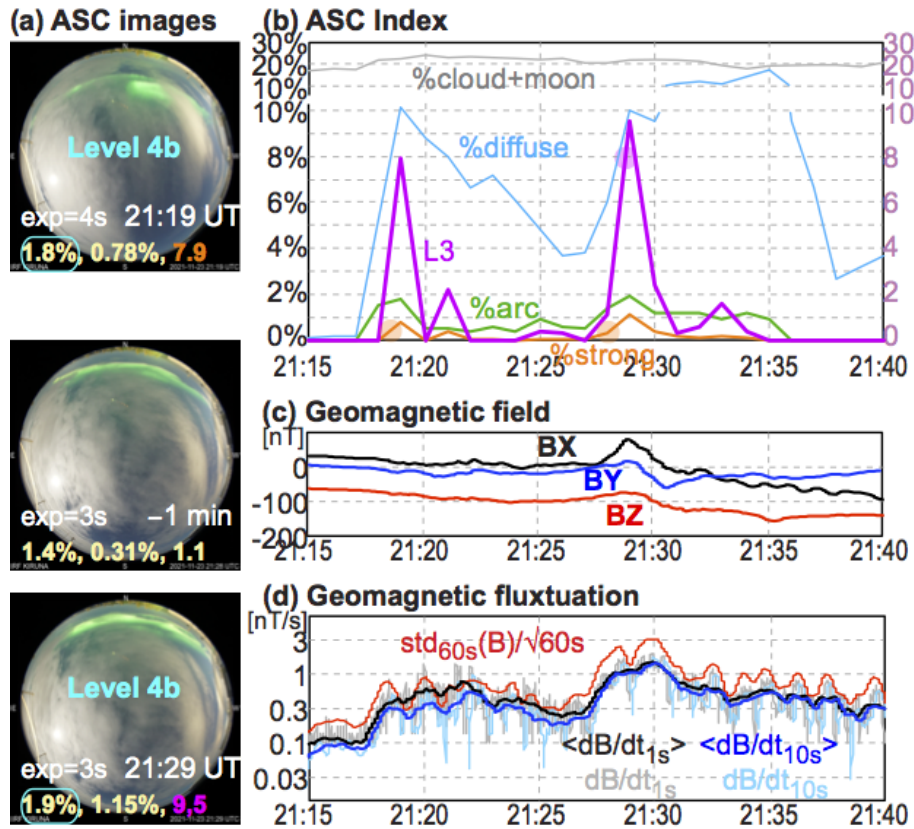
Figure 13. The same as Fig. 8 for the Level 4b auroral activity in the north at 21:29 UT on 23 November 2021.

5 Discussion

We used three categories of aurora instead of two (discrete aurora and diffuse aurora) in section 3.2. Adding a third fuzzy category between two different phenomena is a common practical method in classifying data, and this method is particularly useful here because our aim is to identify the intensification of aurora rather than aurora itself. For the same reason, one may add a new category of "could be aurora" that does not reach the criterion of "visible diffuse" if the purpose is just to identify images that may contain visible aurora, for example, for automated removal of ASC image from the archive (with the condition of no aurora and high cloud coverage).

The present scheme is first automated quantification scheme of real-time auroral activity level, particularly the Local-Arc-Breaking (it is actually in operation even in the 2022/2023 season). It is also the first trial of numerical translation of how the auroral scientists judge the auroral activity (e.g., Akasofu, 1977). Such quantification ability is the main difference from

existing machine-learning schemes (e.g., Nanjo et al., 2022 and references therein): none of them has yet quantified the auroral activity (neither corresponding to ASC auroral index or the activity level).

Several groups have started identification (even classification) of aurora using machine-learning methods (eventually deep learning neural network) directly from ASC images in the RGB colour code (e.g., Clausen and Nickisch, 2018, Kvanmmen et al., 2020; Nanjo et al., 2022, and references therein), and even the real time classification is implemented (Nanjo et al., 2022)[7]. However, what so far exists is only classifying the entire sky into different categories, starting from "training set". For example, Nanjo et al. (2022, Fig. 1) and its reference (Clausen and Nickisch, 2018, Fig. 1) have three auroral categories "arc", "discrete", "diffuse" as one value for each image (here "arc" is scientifically just a special form of "discrete"), but "discrete aurora" and "diffuse aurora" always appears together for all active aurora or during the precursor of active aurora. Also, no machine-learning method has quantified the intensification of the discrete (arc) aurora (at least the authors are not aware of) although such quantification in inevitable in judging the Local-Arc-Breaking. Since most of the auroral images are mixed with cloud (it is very rare to have clear sky during night), the classification of the entire image as one category may often end up "ambiguous" (Clausen and Nickisch, 2018) or "Aurora and cloud" (Nanjo et al., 2022).

Another advantage using the two-step expert system (sets of solid criteria) is that it is relatively easy to pinpoint the reason (by auroral scientists) for any judging error. For example, a masking matrix of $\sim 1.4 \times 10^5$ pixels with true and false values for each category is also stored as a mid-term product for each category before deriving the ASC auroral index. This allows pixel-level examination (cf. Figs. 1c-1e) in case of categorization errors. This method is actually used to separate the cloud effect during the development of the criteria (Tables 2 and 3). We have also identified the reason for the false positive for the moon cases: due to the colour shift of all pixels toward blue by the refraction of the moon light through the all sky dome.

On the other hand, the machine-learning methods may improve or simplify the present method by applying the machine-learning methods to each step (step 1a and step 2) while the logic and aim for each step are kept the same. For example, step 1 may be improved by using the random forest method (Breiman, 2001; Liu et al., 2017) in addition to deep learning. Likewise, the machine-learning method may help improving step 2 only. Inversely, by comparing with the outputs of the present method, improvement of the machine-learning scheme may also become relatively easy.

As the final note, we do not have to change the entire logic but only to adjust the criteria for different ASCs at different locations, although the present criteria are specific for the Kiruna ASC. If the camera and settings are the same, even the present criteria may well be used for the other location. This is because the RGB colour area (particularly R/G ratio for different G range) does not overlap between the non-auroral sources and strong aurora or green arc (present version 1.0 uses only these two categories for activity evaluation). For example, relatively simple cloud identification by Sodium line for Kiruna (589 nm, due to the strong light-pollution by the city), which sometimes has similar hue (H) values as weak aurora, does not alter the identification of the Local-Arc-Breaking very much. Also, difference in the auroral morphology is different at latitudes does not alter the identification of the Local-Arc-Breaking itself very much. At low-latitude stations where the Local-Arc-Breaking occurs in the northward edge, the activity is underestimated due to geometric effect, but the activity in the middle of the sky is still correctly estimated.

---

[7] https://tromsoe-ai.cei.uec.ac.jp/

For different camera manufactures/models that have different colour characteristics, we just need to make different criteria but general colour range must be similar to the present ones. Then, we can aim obtain the similar ASC auroral index values for the same level of activity between different ASC stations.

6 Summary and conclusion

We developed an automatic identification scheme of sudden and significant intensification of auroral arc with expanding motion (Local-Arc-Breaking) seen in the ASC JPEG image that is recorded in the RGB colour code, and applied it for real-time alert. Unlike the other automatic identification trials such as using the deep-learning neural network (none of them has so far quantified the auroral activity), we used a set of simple criteria and calculations (expert system). The scheme is divided into two steps: (1) A set of simple numbers, the ASC auroral index, is defined such that it represents the sky condition of the entire ASC ($\sim 1.4 \times 10^5$ active pixels with a 3 byte colour information each). (2) The auroral activity level is judged only from the index values. The midterm product (ASC auroral index) is stored on real-time bases, whereas the result of activity assessment is sent as warning email real time when the index values satisfy the Level 6 criterion.

The first step is further subdivided into two stages: (1a) pixel-to-pixel classification into "strong aurora", most likely auroral arc (category "green arc"), most likely visible diffuse aurora (category "visible diffuse"), most likely "cloud", most likely "the moon", and most likely "artificial light", using just R, G, B, and hue (H) values (where H is calculated from the RGB values), and (1b) simple calculation such as the percentage of the occupying area (pixel coverage) and the characteristic intensity of the strong aurora (take nonlinear average of luminosity L and L^3 for the most luminous 4900 pixels).

After 5 months of the operation until the end of the 2021/2022 winter season, this algorithm successfully alerted the Local-Arc-Breaking within 10 min from when the actual brightening of aurora is detected for nearly 90% of cases (cf. Table 7). Like the false positive, false negative was also little.

The present scheme is only just version 1.0, and there is a considerable room for improvements. Its direction is clear, thanks to the present method with the explicit criteria and calculations: we need to upgrade the criteria at each step, based on further understanding of, for examples, the camera characteristics against different light sources and relation to the geomagnetic activities (see Appendix B for these tasks).

Appendix A: Version 0 classification using only HSL values

For the old KAGO's ASC (Nikon D700 camera) until April 2020, we used less accurate classification method using only HSL values only to obtain the ASC auroral index version 0 (Yamauchi et al., 2018). In this version, we just plotted the index values in our website in the real-time bases, and its archive is found at the IRF site[8]. For this real time operation, we used criterion (version 0.0) that is summarized in Table A1.

---

[8]https://www.irf.se/maggraphs/aurora_detect/graphs/

Table A1. Version 0.0 criterion of ASC auroral index for old ASC (Nikon D700)

classification Ver.	condition 1 classification	condition 2 H	condition 3 S	L
0.0	strong aurora:	0.20<, <0.46	0.20<, <0.8	0.20<, <0.8
0.0	green arc:	0.18<, <0.46	0.15<, <0.8	0.10≤, <0.8
0.0	visible diffuse:	0.16<, <0.50	0.10<, <0.8	0.5≤, <0.8
0.0	cloud:	< 0.16	0.10<, <0.8	0.15<, <0.8
0.1	strong aurora:	0.20≤, <0.46	0.17≤, <0.8	0.30≤, <0.83
0.1	green arc:	0.18≤, <0.46	0.13≤, <0.8	0.15≤, <0.83
0.1	visible diffuse:	0.16≤, <0.57	0.09≤, <0.8	0.5≤, <0.83
0.1	cloud:	<0.16	0.10≤, <0.8	0.15≤, <0.83
0.1	moon:		<0.13	0.75≤, ≤1

This version (version 0.0) was slightly updated for the data analyses when the operation of the old ASC (Nikon D700 camera) is finished. The revised criterion (version 0.1) is summarized in the same table.

Appendix B: Future improvements

In Appendix B, we list tasks for future improvement that we consider feasible, in addition to tuning the criterion values (e.g., 2.8% instead of 3.0% for %arc in the Level 6 criterion, etc.).

These improvements require further subdivision of auroral image (e.g., different local times, different exposures, different aurora with moon, etc.), and hence, require more auroral examples to examine than what we examined so far.

B1 Correction using exposure time information (for step 1) and UT information (for both steps)

The present version is made to judge only from the JPEG image, but not using hidden information, such that the analyses code (see supplemental material) can be easily modified for the other ASC images, e.g., taken at non-scientific station (Toyomasu et al., 2008). However, we can use two extra information that are available in the most JPEG images. One is the UT information that is tagged to the ASC images in most of the places. The other is the exposure time given as hidden information of the JPEG file (can be extracted with, e.g., "exiftool" command, for python program). Although the present version identifies most of the Local-Arc-Breaking for different UT and for different exposure time, including these information will further improve both the ASC auroral index and activity level definition. For example, post-midnight diffuse aurora during a substorm is often too strong and misjudged as the auroral arc (category "green arc") although such an overestimation does not affect judging Level 6 and Level 4b very much.

B2 N_2 red (670 nm) line (for step 1)

In the present version, all aurora pixels must satisfy R<G and B<G (the same as $0.167 \leq H < 0.5$) to avoid any contamination from white light or twilight. This automatically removes the strong red emission by N_2 around 670 nm (mainly < 100 km altitudes) shown in Fig. 4b, or faint blue emission by N_2^+ at 428 nm (mainly > 150 km altitude). Adding these lines, particularly the strong N_2 red line, would improve the "strong aurora" definition. Fortunately, N_2 red line in Fig. 4b does not belong to any category yet, opening up a possibility to add a new category "N_2 aurora". To add this category, we must examine more examples with strong N_2 red lines (they are rare) to find out the relevant RGB colour code while limiting to the RGB colour range different from the twilight, moon, and other light sources. Priority is lower for extracting the N_2^+ blue line than the N_2 red line because the N_2^+ blue line appears more often near the equinoxes than winter, and including the N_2^+ blue line may cause inequality between different seasons.

B3 Moon filter and twilight filter (for step 1)

To reduce the moon effect, we currently mask all pixels within a radius that is 14 times the detected moon radius (even the radius of the moon changes with time, location, and moon phase) because both the sky and the all-sky dome scatters the moonlight, modifying the colour and intensity of the aurora pixels in a wide area around the moon during almost all moon phases. Of course the moon itself blocks the aurora at its vicinity.

Just masking the moon from date and time is not practical because the all-sky dome modifies the moon location and size. Also, the effect (shift of the colour toward blue) is seen at almost all pixels of the entire image, with higher effect at closer to the moon. One possible counterpart is to use "corrected B" values that are reduced from the obtained B values, depending on the distance from the moon. The goal is to make the similar values of the ASC auroral index (for strong aurora and green arc, at moment) for the same level of aurora between with and without the moon. We can make the similar correction for the twilight, but this is not as urgent as the moon correction because the twilight problem is seen only at the beginning and end of the season when the night is very short.

B4 Defining less intense but sudden intensification as Level 5 (for step 2)

Some Local-Arc-Breakings are more compact and less intense than others. Some of them are even difficult to distinguish from simple intensification or deformation of auroral arcs, e.g., expansion of bright region or only nearly breaking that soon returns to the green arc again. Therefore, it would be useful to have a category of minor sudden intensification as Level 5. Such introduction of "fuzziness" makes the alert system more reliable.

B5 Dividing field-of-view (for both steps)

The present ASC auroral index treats all pixels equal, which makes the zenith aurora weighted more in the calculation of the index values than the other part of the sky due to the physical geometrical effect while another type of weighting is introduced by the fish-eye lens' optical geometry. Furthermore, the Local-Arc-Breaking in the south sky expands toward the entire sky

(Akasofu, 1977), giving higher values than the Local-Arc-Breaking in the northern sky that expands mainly toward northern edge. These "auroral location" problems (reliable only near the zenith or slightly south) should ideally be solved by placing many ASCs within 100 km distance each other. Meanwhile, we can make some improvement with a single ASC by dividing the field-of-view into two-three areas (north, middle, south) and obtaining the index values for each area, in addition to introducing simple correction that depends on the zenith angle. When calculating the final index values, we can weight differently between there three regions (more weight for the northern sky than southern sky).

B6 Previous 5-min activities (for step 2)

For some Local-Arc-Breaking cases without the Level 6 alert, its criterion is satisfied if we take peak values of the ASC auroral index within 5 minutes (4 cases in 2022 out of 8 nights in Table 7: On 8 Feb, 7 March, 12 March, and 3 April). These examples suggest a possibility to loosen the criterion by using nearby data. Other possible solution is to introduce gradients of values such that sharp increases of %strong and L3 as the condition to ease the criterion. Such attempts are also useful in defining Level 5 (less intense auroral intensification) and lower level of activities. Problem is that the optimization requires complicated examinations of multi-minutes data, and finding the solution is not simple. This could be a good task to use the machine-learning methods for optimization.

B7 Precursor or Level 4 (for step 2)

As the extension of the previous task (considering previous 5-min activity), we can even search precursor signatures of the Local-Arc-Breaking. Level-4a and Level-4b are defined as the first step for this effort, and the methods mentioned above (including machine-learning methods) will help tuning Level 4. In case of using the machine-learning method, only the ASC auroral index values during past 10 minutes should be used to predict Level 6 activity without examining the image data. Then, we can define the ASC auroral index values between 5 min before the Level 6 and 10 min before the Level 6 can be a good candidate of set of values corresponds to Level 4.

B8 Adding geomagnetic variation (for both steps)

As an external index, local geomagnetic activity can be used to help defining the level (cf., Juusola et al., 2020). To evaluate the optimum information for this purpose, we showed geomagnetic variations in Figs. 7-11, and 13 in both DC and AC formats. As the AC variation, we showed $|d\mathbf{B}/dt|$ values obtained from the 1s resolution values and from 10s resolution values, and their 1-min running averages, respectively. We also showed theoretical accuracy of the 1s resolution values, i.e., standard deviation divided by square root of 60s, giving the result with the same unit [nT/s] as other parameters.

Change in B_X (deviation within 10 minutes or so) is the optimum parameter for DC variation, whereas all AC profiles are similar to each other, suggesting that using 10-sec values is sufficient as the source data when 1s resolution data is not available. On the other hand, the standard deviation method might be optimum if the computation time is short enough. This problem

is directly related to the geomagnetically induced current (GIC) during the spaceweather hazard events. That is, we can even search for possible precursor of the big GIC events (big $|d\mathbf{B}/dt|$ events) in the ASC auroral index.

Code availability. Python code is found in the supplemental material (except sending email alert part which includes private information)

555 *Data availability.* The all sky images and magnetic field data are publicly available at IRF's observatory data site https://www.irf.se/en/about-irf/data/, with ASC data at https://www.irf.se/alis/allsky/krn/, magnetic field data at https://www.irf.se/maggraphs/iaga/, and ASC auroral index at https://www.irf.se/alis/allsky/nowcast/.

Author contributions. MY is responsible all part except the calibration, maintenance and optimum setting of the ASC, for all of which UB is responsible

560 *Competing interests.* no competing interest

Acknowledgements. The work is partially funded under ESA contract number 4000134036/21/D/MRP as part of the ESA Space Safety Programme and by the EU projectRIT (Space for innovation and growth) with the objective of developing the space region in northern Sweden. Maintenance of system including software is done by members of Kiruna Atmospheric and Geophysical Observatory (KAGO) at IRF. We also thank Dennis van Dijk for developing preliminary version (version 0) made for the old Nikon D700 camera, and Arnau Busom
565 i Vidal for examining the Local-Arc-Breaking.

References

Akasofu, S.-I.: The development of the auroral substorm, Planet. Space Sci., 12, 273-282, https://doi.org/10.1016/0032-0633(64)90151-5, 1964.

Akasofu, S.-I.: Physics of magnetospheric substorms, Astrophysics and space science library, vol. 47, Reidel, Dordrecht, https://doi.org/10.1007/978-94-010-1164-8, 1977.

Brändström, B. U. E., Enell, C.-F., Widell, O., Hansson, T., Whiter, D., Mäkinen, S., Mikhaylova, D., Axelsson, K., Sigernes, F., Gulbrandsen, N., Schlatter, N. M., Gjendem, A. G., Cai, L., Reistad, J. P., Daae, M., Demissie, T. D., Andalsvik, Y. L., Roberts, O., Poluyanov, S., and Chernouss, S.: Results from the intercalibration of optical low light calibration sources 2011, Geosci. Instrum. Method. Data Syst., 1, 43-51, https://doi.org/10.5194/gi-1-43-2012, 2012.

Breiman, L.: Random Forests. Machine Learning 45, 5-32, https://doi.org/10.1023/A:1010933404324, 2001

Friis-Christensen, E., McHenry, M. A., Clauer, C. R., and Vennerstrom, S.: Ionospheric traveling convection vortices observed near the polar cleft: a triggered response to sudden changes in the solar wind, Geophys. Res. Lett., 15, 253-256, https://doi.org/10.1029/GL015i003p00253, 1988.

Helmholtz - German Research Centre for Geoscience (GFZ) in Potsdam, Real-time Kp, https://isdc.gfz-potsdam.de/kp-index/

Juusola, L., Vanhamäki, H., Viljanen, A., and Smirnov, M.: Induced currents due to 3D ground conductivity play a major role in the interpretation of geomagnetic variations, Ann. Geophys., 38, 983-998Ann. Geophys., 38, 983-998, https://doi.org/10.5194/angeo-38-983-2020, 2020.

Kvammen, A., Wickstrøm, K., McKay, D., and Partamies, N.: Auroral image classification with deep neural networks. J. Geophysi. Res., 125, e2020JA027808, https://doi.org/10.1029/2020JA027808, 2020.

Liu, C., Deng, N., Wang, J.T.L. and Wang, H.: Predicting solar flares using SDO/HMI vector magnetic data products and the random forest algorithm, Astrophys. J., 843, 104, https://doi.org/10.3847/1538-4357/aa789b, 2017.

Luhr, H., Aylward, A., Bucher, S.C., Pajunpaa, A., Pajunpaa, K., Holmboe, T., and Zalewski, S.M.: Westward moving dynamic substorm features observed with the IMAGE magnetometer network and other ground-based instruments, Ann. Geophys., 16, 425-440,. https://doi.org/10.1007/s00585-998-0425-y, 1998.

Nanjo, S., Satonori Nozawa, S., Yamamoto, M., Kawabata T., Johnsen,M.G., Tsuda, T.T, Hosokawa, K.: An a auroral detection system using deep learning: real-time operation in Tromsø, Norway, Sci. Rep., 12, 8038, https://doi.org/10.1038/s41598-022-11686-8, 2022.

Partamies, N., O. Amm, K. Kauristie, T. I. Pulkkinen, and E. Tanskanen, A pseudo-breakup observation: Localized currentwedge across the postmidnight auroral oval, J. Geophys. Res.,108(A1), 1020, 10.1029/2002JA009276, 2003.

Sigernes, F., Holmen, S. E., Biles, D., Bjørklund, H., Chen, X., Dyrland, M., Lorentzen, D. A., Baddeley, L., Trondsen, T., Brändström, U., Trondsen, E., Lybekk, B., Moen, J., Chernouss, S., and Deehr, C. S.: Auroral all-sky camera calibration, Geosci. Instrum. Method. Data Syst., 3, 241-245, https://doi.org/10.5194/gi-3-241-2014, 2014.

Syrjäsuo, M.T., Pulkkinen, T.I., Janhunen, P., Viljanen, A., Pellinen, R.J., Kauristie, K., Opgenoorth, H.J., Wallman, S., Eglitis, P., Karlsson, P., Amm, O., Nielsen, E., and Thomas, C.: Observationsof substorm electrodynamics using the MIRACLE network, in Substorms-4, edited by Kokubun S., and Kamide, Y.,Terra Scientific Publishing Company, Tokyo, 111-114, 1998

World data center (WDC) in Kyoto, Real-time AE, https://wdc.kugi.kyoto-u.ac.jp/ae_real-time/presentmonth/index.html

Yamauchi, M., Brandstrom, U., van Dijk, D., Sergienko, T., and Kero, J.: Improving nowcast capability through automatic processing of combined ground-based measurements, in EGU General Assembly Conference Abstracts, p. 1779, 2018.